ACS NANO
Cite This: ACS Nano 2017, 11, 12111−12120
www.acsnano.org

ARTICLE

The Molecular Mechanism of Nanodroplet Stability

Evangelia Zdrali,[†] Yixing Chen,[†] Halil I. Okur,[†] David M. Wilkins,[‡] and Sylvie Roke*[,†]

[†]Laboratory for Fundamental BioPhotonics, Institutes of Bioengineering and Materials Science and Engineering, School of Engineering, and Lausanne Centre for Ultrafast Science, École Polytechnique Fédérale de Lausanne (EPFL), CH-1015 Lausanne, Switzerland

[‡]Laboratory of Computational Science and Modeling, Institute of Materials, École Polytechnique Fédérale de Lausanne, 1015 Lausanne, Switzerland

Supporting Information

ABSTRACT: **Mixtures of nano- and microscopic oil droplets in water have recently been rediscovered as miniature reaction vessels in microfluidic environments and are important constituents of many environmental systems, food, personal care, and medical products. The oil nanodroplet/water interface stabilized by surfactants determines the physicochemical properties of the droplets. Surfactants are thought to stabilize nanodroplets by forming densely packed monolayers that shield the oil phase from the water. This idea has been inferred from droplet stability measurements in combination with molecular structural data obtained from extended planar interfaces. Here, we present a molecular level investigation of the surface structure and stability of nanodroplets and show that the surface structure of nanodroplets is significantly different from that of extended planar interfaces. Charged surfactants form monolayers that are more than 1 order of magnitude more dilute than geometrically packed ones, and there is no experimental correlation between stability and surfactant surface density. Moreover, dilute negatively charged surfactant monolayers produce more stable nanodroplets than dilute positively charged and dense geometrically packed neutral surfactant monolayers. Droplet stability is found to depend on the relative cooperativity between charge−charge, charge−dipole, and hydrogen-bonding interactions. The difference between extended planar interfaces and nanoscale interfaces stems from a difference in the thermally averaged total charge−charge interactions in the two systems. Low dielectric oil droplets with a size smaller than the Debye length in oil permit repulsive interactions between like charges from opposing interfaces in small droplets. This behavior is generic and extends up to the micrometer length scale.**

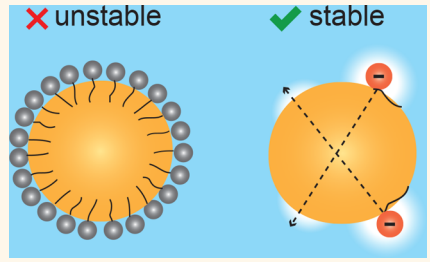

KEYWORDS: *nanodroplets, stability, interface, water, sum frequency scattering, charge, screening*

Mixtures of nano- and microscopic oil droplets in water or water droplets in oil are known as emulsions.[1−3] Emulsions are widely applied in technological applications, as food products, agrochemical compounds, drugs, and paints, among others. Recently, droplets in microfluidic systems have found new applications, such as minuscule reaction vessels[4−9] useful for drug screening,[10] analysis of biomolecules,[11] and cell screening.[12,13] In these emulsions the droplets are kinetically stable, which means that eventually the system will phase-separate into an oil and a water phase, driven by processes such as flocculation, coalescence, and Ostwald ripening.[1,2] The stability of droplets can be increased by surfactants that alter the interfacial structure and thereby create an interface with a minimal free energy. In order to achieve better control over droplet systems and their applications, it is important to understand the molecular mechanism behind droplet stability. To do so, molecular interfacial structural information needs to be correlated with droplet stability data. This is typically done[14−17] by correlating surface structural data from extended planar interfaces, such as that gathered from X-ray,[18−20] neutron scattering/reflection,[21,22] and sum frequency generation (SFG)[23−28] studies, to stability data of droplets made of the same chemicals as the planar systems. These studies show that surfactants lower the interfacial energy of macroscopic planar interfaces by forming a densely packed (geometric) monolayer. However, recent reports[29−33] show that the curved interfaces of droplets do not display the same molecular structure as planar extended interfaces. Simple geometrical packing[14] is insufficient to explain interfacial amphiphile structure. For example, sodium dodecyl sulfate was found to form very dilute monolayers on nanodroplets that differ in density from the corresponding planar interfaces by at least an

Received: July 19, 2017
Accepted: December 10, 2017
Published: December 11, 2017

ACS Publications © 2017 American Chemical Society

DOI: 10.1021/acsnano.7b05100
ACS Nano 2017, 11, 12111−12120

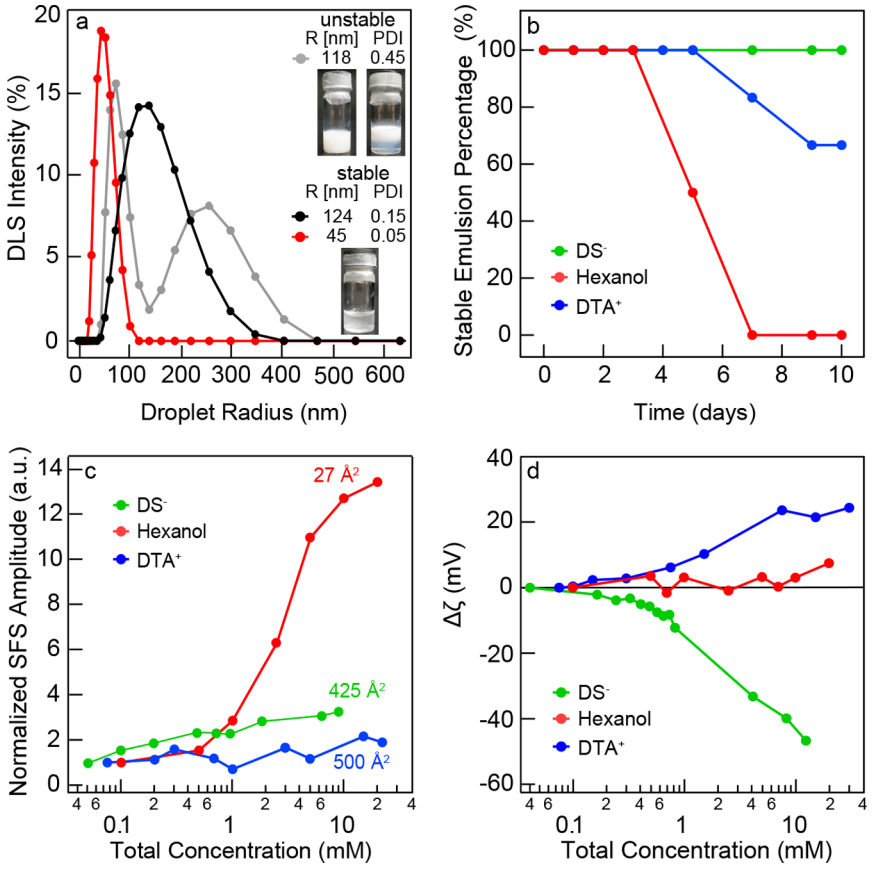

Figure 1. Stability and surface group density. (a) Three typical droplet size distributions of stable (red and black) and unstable (gray) droplets as determined by DLS. The inset displays photographs of stable and unstable samples. Note that the *x*-axis has a linear scale. (b) Percentage of samples that remain stable as a function of time. Each sample consists of 1 vol % hexadecane (99.8% pure) nanodroplets in ultrapure water with 150 μM SDS, DTAB, or hexanol. (c) SFS amplitude, which is proportional to the surfactant surface density, as a function of total surfactant concentration in the sample. The calculated minimum area per molecule for the maximum concentration (in Å^2) is given for each surfactant. The SFS spectra were collected with the infrared (visible, sum frequency) beam polarized parallel (perpendicular) to the scattering plane (SSP) and recorded for the S−O symmetric stretch mode (~1080 cm^{-1}) for DS$^-$ and for the C−H stretch modes (~2900 cm^{-1}) for DTA$^+$ and hexanol. SFS amplitudes are normalized with the DLS size distribution according to the protocol in ref 34. (d) Change in the droplets' ζ-potential as a function of total surfactant concentration.

order of magnitude,[29] the water molecules at the surface of water droplets in a hydrophobic liquid are much more ordered than water molecules at identical planar/water interfaces,[30] and liposomes exhibit transmembrane asymmetry in their hydrating water rather than in their lipid distribution.[34] These findings were made employing vibrational sum frequency scattering (SFS)[35,36] and angle-resolved[37] second-harmonic scattering (SHS)[36,38] techniques that probe the molecular structure of the oil, the water, and the surfactant on nanodroplet/particle surfaces in aqueous solution.[39] Vibrational SFS is a coherent surface spectroscopy that provides information on chemical composition, molecular order, and orientation of interfacial molecules present on droplets or particles.[29,40,41] Nonresonant angle-resolved SHS is a probe of the orientational order of interfacial water molecules: It reports on the difference in orientational directionality between interfacial water molecules and bulk water molecules.[42,43]

Here we provide a systematic investigation of the macroscopic stability, the molecular structure, and the relevant interactions for oil droplets in aqueous solutions. In order to produce smooth, defect-free interfaces, we use ~100 nm in radius hexadecane oil droplets stabilized with neutral (alkanols and zwitterionic lipids), positively charged (dodecyltrimethylammonium bromide, DTAB), or negatively charged (sodium dodecyl sulfate, SDS) amphiphiles. These chemicals are chosen such that they represent different charges with and without hydrogen bonding in contact with a water/dielectric nanoparticle interface. We present stabilizing performance, charging, hydration, and surface density data of the amphiphilic molecules as well as structural information on the interfacial oil and interfacial water molecules. Finally, the combined data are broken down in terms of relevant interactions, and a mechanism relevant for surface structure and stability is proposed, which differs from the framework used for planar interfaces. We observe that high droplet stability does not necessarily require a high surface charge density but rather a sufficient amount of surface charge and cooperativity between hydrogen bonding and charge−dipole interactions. The nano/submicrometer size of the droplets, in combination with a lack of conducting species in the oil phase, results in nonzero repulsive interactions between the surface charges on opposite sides of the droplet. This interaction is absent for neutral/zwitterionic droplet surfaces and limits the surface charge density to one that is lower compared to equivalent planar interfaces. This proposed mechanism is supported by a simple electrostatic model that captures the essence of the relevant

DOI: 10.1021/acsnano.7b05100
ACS Nano 2017, 11, 12111−12120

physics, as well as surface charge density measurements as a function of ionic strength.

RESULTS AND DISCUSSION

Stability. To quantify droplet stability, nanodroplets were prepared with 150 μM of either SDS (critical micelle concentration, cmc, of 8.25 mM at T = 293 K),[44] DTAB (cmc of 15.9 mM at T = 293 K),[44] or hexanol (solubility of 65 mM at T = 293 K).[45] The preparation procedure can be found in the Materials and Methods section. With the chosen low concentration of surfactants the destabilization process occurs within a time frame of several days. The stability was determined by a standard protocol[2] of visual inspection and size distribution measurements. The droplet size distribution was measured over 10 days with dynamic light scattering (DLS). The droplet size distribution of freshly prepared samples consists of a single peak centered at a radius R in the range 45 < R < 125 nm (see Figure 1a, red and black, for two size distributions representative of the range of samples that have been prepared) with a polydispersity index (PDI) of 0.05 < PDI < 0.25. These values are typical for nanoemulsions.[3] The nanodroplets were considered unstable[2] if (i) there was a phase separation, (ii) new peaks appeared in the size distribution (see Figure 1a for an example in gray), and/or (iii) the PDI became larger than 0.3, or (iv) the droplet size increased by more than 15% over a time span of 10 days. Each measurement was performed three times on each sample. Figure 1b displays the percentage of samples that remained stable over time, measured up to 10 days after their preparation. Here it can be seen that the dodecylsulfate ion (DS^-) is the best stabilizer, as all samples remained stable for at least 10 days. The dodecyltrimethylammonium (DTA^+) ion follows, with 30% of the samples becoming unstable after 5 days. All hexanol nanodroplets were destabilized after 7 days, suggesting that hexanol is the least effective stabilizer of the three representative surface active compounds studied here. Further data are summarized in Table 1.

Table 1. Stability and Interfacial Structure: A Summary of the Characteristics of the Studied Hexadecane-in-Water Nanodroplets

component	stability (days)	min. surface area/molecule (nm^2)	interfacial water alignment	interfacial oil structural changes
DS^-	>10	>4.25	increases	not detectable
DS^- + 30 mM NaCl	>10	>2.13	increases	not detectable
DTA^+	<5	>5.00	vanishes	more chain disorder
hexanol	<3	0.27	decreases	more chain disorder
dodecanol	<3	0.27	decreases	more chain disorder
DPPC	<3	0.48	decreases	more chain disorder

Surface Density. The surface density of amphiphiles can be derived from SFS spectral amplitudes, recorded from nanodroplets that contain the same droplet size distribution but a different total surfactant concentration.[29] With an identical size distribution and an average surfactant orientation that is not changing over the probed concentration range, a change in the SFS amplitude is proportional to a change in surface density.[29,46] Figure 1c shows the relative amplitude change for the interfacial S−O symmetric stretch mode of DS^- anions and the C−H stretch modes of DTA^+ cations and hexanol molecules. It can be seen that, over the same concentration range, the relative increase of the surface density of hexanol is much larger (×13) than those of the two ionic surfactants (×2 for DTA^+ and ×3 for DS^-). The maximum surface density (or minimum projected surface area) of each amphiphile can be retrieved by assuming that, as an upper limit, for the lowest total concentration (*e.g.*, 55 μM for SDS or 100 μM for DTAB) all surfactant molecules are adsorbed at the interface. Without this assumption the retrieved surface density values will be even lower. In addition, it is possible to use a modified Langmuir adsorption model to estimate the surface density of amphiphiles.[47] Using these procedures we found the lower limit for the projected surface area per molecule of hexanol (27 ± 7 Å^2),[46] DS^- (>425 Å^2),[48] and DTA^+ (>500 Å^2). The surface density of hexanol is at least an order of magnitude higher than those of the two ionic surfactants. Dodecanol was shown to have a surface density very similar to that of hexanol,[46] with 29 ± 5 Å^2 per molecule. These experimental findings suggest that the adsorption behavior of amphiphiles, as well as the resulting droplet stability, is related to their charge, rather than their molecular packing. This notion is supported by the fact that the observations are done for a distribution of different sizes and PDIs and that curvature-related packing differences are most commonly found in systems smaller than ∼50 nm.[49]

Charge. A commonly used indicator for droplet stability is the electrokinetic mobility of particles in aqueous solutions,[2] which is reported on by the ζ-potential.[50] Higher stability is generally achieved with a higher ζ-potential amplitude, which results in efficient droplet repulsion, thereby preventing coalescence that leads to instability.[1] Figure 1d shows the change in the ζ-potential of hexadecane nanodroplets in water with increasing concentrations of SDS, DTAB, and hexanol. The ζ-potential changes with different magnitudes as the DS^- and DTA^+ concentrations increase in the solutions. Increasing the surfactant concentration from ∼75 μM to ∼10 mM results in a change of −40 mV for SDS, while only ∼20 mV is added to the initially positive ζ-potential of droplets in DTAB solutions. Hexanol-stabilized droplets do not have a different ζ-potential than pure oil droplets in water. Comparing the DTA^+- and DS^--stabilized droplets, we find that the more stable nanodroplets have a higher surface density and a bigger relative change in the ζ-potential. The surface density ratio of DS^- and DTA^+ ions (×1.3 at 10 mM) correlates well with the $\Delta\zeta$-potential ratio of DS^- and DTA^+ (×1.8 at 10 mM). Nanodroplet stability is thus clearly correlated with the amount of surface charge, which is in agreement with expectations.[1] The increase of surface charge can explain the stability achieved by the addition of ionic surfactants; however, it does not explain the case of hexanol or the low surface densities that are found for the charged surfactants. For further understanding of the relationship between surface stability and surface molecular structure we revisit derived structural changes of the oil and water molecules, as well as the bulk hydration characteristics for the three systems.

Molecular Interfacial Structure and Bulk Hydration. The structural changes imposed by the amphiphiles on the interfacial oil molecules are reflected in the SFS spectra of the C−H stretch modes of hexadecane droplets dispersed in D_2O (Figure 2a), in which the bulk concentrations of deuterated $(d)_{25}$-SDS (0.98 × cmc), d_{34}-DTAB (0.93 × cmc), or d_{13}-

DOI: 10.1021/acsnano.7b05100
ACS Nano 2017, 11, 12111−12120

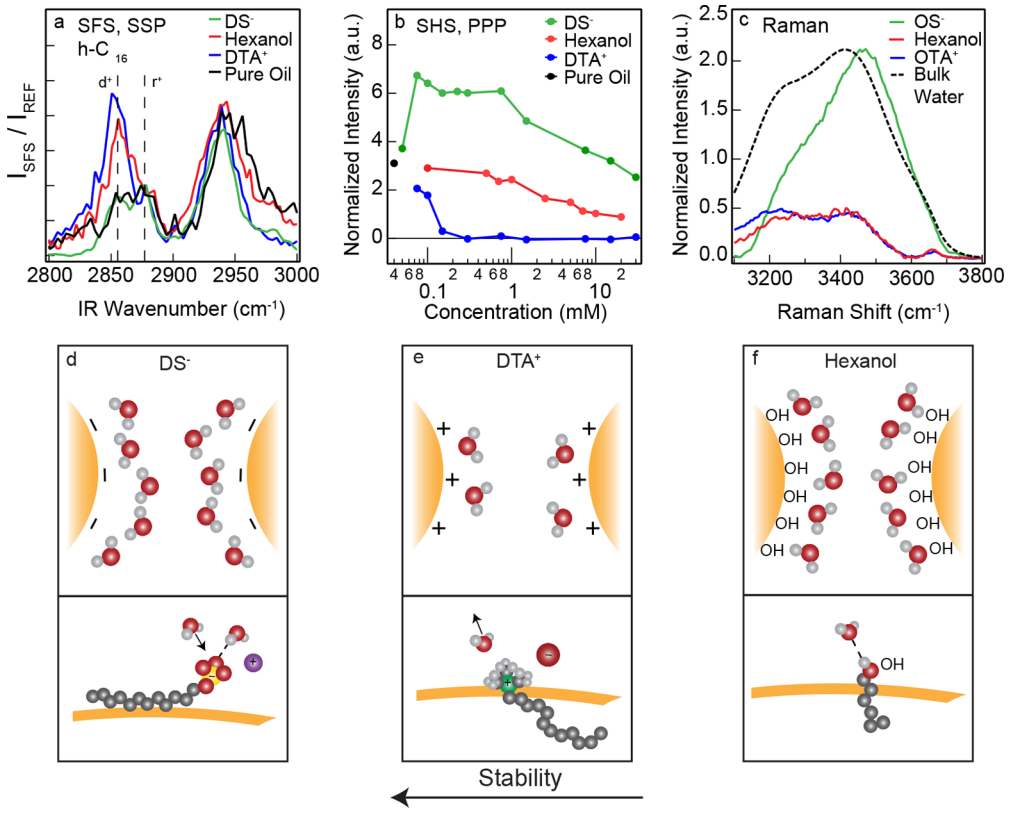

Figure 2. Interfacial structure and bulk hydration. (a) Normalized SFS spectra of the C−H stretch modes of hexadecane droplet interfaces stabilized with d_{25}-DS^- (8 mM, green), d_{34}-DTA^+ (12 mM, blue), or d_{13}-hexanol (5 mM, red). The SFS spectrum of pure oil nanodroplets in water is also shown (black). The SFS spectra were collected in the SSP polarization combination. (b) SHS intensity, recorded with all beams polarized in the horizontal plane, at a scattering angle of 35°, of a 0.1 vol % d_{34}-hexadecane/water nanoemulsion stabilized with hexanol, SDS, or DTAB as a function of the amphiphile concentration. The intensity of the SFS and SHS measurements is normalized using an effective droplet radius retrieved from the DLS size distribution according to the protocol in ref 34. Intensities are therefore independent of droplet radius and size distribution. (c) Raman hydration shell spectra of 100 mM aqueous solutions of octylsulfate anions (OS^-), octyltrimethylmmonium cations (OTA^+), and hexanol molecules. The spectra display the O−H stretch vibrational response of the water surrounding the surfactant ions. The O−H Raman spectrum of pure water (black) is also presented and scaled to the same height as the OS^- hydration-shell O−H band. (d−f) Schematic diagrams of the influence of the surfactant's surface structure of the systems measured in (a) and (b). The dashed lines represent hydrogen bonds, and the arrows represent dipole moments. The bottom panels display the primary interaction(s) of a surfactant molecule with the interfacial water molecules. (d) A DS^- ion influences the water orientation with respect to the interface through both hydrogen-bonding and electrostatic interactions. (e) A DTA^+ ion influences the water orientation with respect to the interface through electrostatic interactions only. (f) A hexanol molecule influences the water orientation with respect to the interface through hydrogen bonding only. The top panels illustrate the relationship between the molecular interactions and the interactions that take place when droplets approach each other, which relates to droplet stability.

hexanol were different.[51] Using selective deuteration, the vibrational modes of the surfactant are removed from the SFS spectral window, allowing independent probing of the structural changes of the oil surface. Compared to pure hexadecane droplets in water, it can be seen that DS^- ions do not significantly alter the conformation of oil molecules, as they leave the vibrational spectrum unchanged. The same behavior is observed for oil droplets made of dodecane and hexane.[48] In contrast, DTA^+ and hexanol cause a significant change in the interfacial vibrational spectrum and, hence, are concluded to perturb the interfacial oil structure.[51] Analysis of these spectral changes resulted in a structural interpretation that has the DTA^+ and the hexanol molecules penetrating into the oil phase, while the DS^- molecules lie flat on the oil surface without much interaction.[48,51,52] Figure 2b displays the change in the SHS intensity of 100 nm (radius) hexadecane droplets in water as a function of the surfactant concentration (published previously in refs 29 and 46). These data show that the orientational order of interfacial water is altered when the amount of surfactant is increased. The change is also different for each surfactant: DS^- increases the water order, while DTA^+ decreases the water order, and hexanol induces a smaller loss in water order than DTA^+. This behavior differs significantly from what is expected for geometrical packing and can be explained by the interplay of the different interactions:[53] For negatively charged interfacial DS^- ions, both hydrogen bonding and charge−water dipole interaction require water molecules to be oriented predominantly with their hydrogen atoms toward the interface. However, for a positively charged DTA^+-covered interface, there is little hydrogen bonding and the charge−dipole interaction is orienting the interfacial water molecules oppositely. Hexanol, on the other hand, induces a decrease in the directionality of water along the surface normal, which is caused by the formation of hydrogen bonds between the OH group of hexanol and the interfacial water molecules. This decrease in the directionality of water matches with the increasing surface density of hexanol as the concentration of hexanol in the solution is increased (see also ref 46). Figure 2c

DOI: 10.1021/acsnano.7b05100
ACS Nano 2017, 11, 12111−12120

shows the Raman hydration shell spectra of the O−H stretch region of 0.1 M solutions of octylsulfate (OS^-) anions, octyltrimethylammonium (OTA^+) cations,[29] and hexanol molecules.[54] The hydration shell spectra represent the spectral difference in Raman intensity between a solute/solvent mixture and the pure solvent. The spectral content is explained as the differential vibrational response of the hydration shell and bulk water. Thus, it reports on solvent−solute interactions that are different from those in bulk water.[55] For these measurements octyl alkyl chains were chosen instead of dodecyl so as to exploit the higher cmc concentrations of >100 mM[44] for sodium octylsulfate (SOS) and octyl trimethylammonium bromide (OTAB) (enabling spectral recordings with a better signal-to-noise ratio). The influence of counterions was eliminated.[51] Compared to bulk water, the three hydration shell spectra are different, with hexanol and OTA^+ cations having a similar, more red-shifted, spectrum and the OS^- anions having a more intense and blue-shifted spectrum. The red shift can be interpreted as a sign of enhanced tetrahedral ordering of water molecules around the OTA^+ ions and hexanol molecules.[46,51] The hydration shell spectrum of OS^- anions was interpreted to have more, but weaker, hydrogen bonds between water molecules around OS^- than in an identical volume of pure water.[51] This difference in hydration matches well with the different interfacial water ordering of Figure 2b. The rearrangement of interfacial water molecules around DTA^+ and hexanol, due to electrostatic and hydrogen-bonding interactions, respectively, disrupts the already existing water ordering, resulting in a decrease in the SH intensity. In the case of DS^-, the large increase observed in the SH intensity is due to hydrogen-bonding and electrostatic field interactions, which both result in more orientational order of water along the surface normal. The subsequent decrease (>1 mM) arises from the screening of the surface electrostatic field by the counterions, resulting in less ordered water molecules.

Figure 2d−f are indicative illustrations of the interfacial structure of the three systems studied here, allowing a structural comparison. The surface density of the interfacial ions (DS^- in Figure 2d, DTA^+ in Figure 2e) or hexanol molecules (in Figure 2f), as well as the respective orientation of the interfacial water molecules, are displayed in the top panels. The bottom panels show the interaction of the amphiphiles with the interfacial oil layer and interfacial water molecules in more detail. In the following we discuss the correlation between the interfacial structure of these three exemplary systems and the observed droplet stability.

Stability and Structure. For a geometrical interfacial packing, with all structure-determining interactions being nonspecific, no difference in the emulsion stability between DS^-, DTA^+, and hexanol would be expected. Similar saturated surface densities and similar changes to the respective interfacial oil and water structures for all three surfactants would be expected. In nanoscale systems, an increasing curvature ($R\downarrow$) is typically interpreted as leading to an increase in available volume per interfacial molecule and thus an increase in surface density. This behavior very strongly depends on the actual curvature and becomes important on metal and high-dielectric particles or when surfactants are paired with counterions.[49,56]

Combining all stability and structural findings in Table 1, we find a very different picture than the one suggested by geometrical packing. Instead, a distinct trend in stability dependent on surface chemistry, a very low surface density for the charged surfactants, and specific changes in the oil/water structure per surfactant are observed. In addition, in contrast to expectations for geometrical packing, we observe the same behavior for a rather large variety of sizes (45 nm < R < 125 nm) and distributions 0.05 < PDI < 0.25 for the 25 different samples that were prepared and probed here.

Based on these many differences, it seems necessary to re-evaluate the effect of curvature and consider that a balance of interactions is responsible for the stability of the nanodroplets. For hexanol, nanoemulsions are stable only for several days. The repulsion between the droplets is therefore probably weak (in the absence of any interfacial ionic species), but the oriented interfacial water molecules (see Figure 2f) present an oriented layer of dipoles which does provide dipolar electrostatic repulsion. Moving upward in stability with DTA^+, there is a dilute layer of charges at the interface (Figure 2e), which results in positively charged droplets that repel each other.

The positive charges are screened by the counterions and by oriented water dipoles, but there are no hydrogen bonds between DTA^+ and the interfacial water molecules. For DS^-, in addition to charge−charge repulsion and screening by counterions and water dipoles, there is a population of oriented water molecules that form hydrogen bonds with the sulfate head groups (Figure 2d). The charge of the DS^- ions thus experiences a more thorough screening than that of the DTA^+ ions, which is reflected in the lower surface density and lower ζ-potential change of DTA^+ compared to DS^- (Figure 1c,d).

That the surface density of DS^- and DTA^+ is much lower than what is expected based on planar surface experiments[25,57] can then be explained by considering interactions rather than excluded volume. The interaction between charged molecules in a solution is determined by a balance of Coulombic interactions between ions and their thermal motion. The Debye screening length ($1/\kappa$) provides an indication for the distance over which ions are separated in a liquid.[16] The electrostatic potential has decayed to ∼2% of its value after a distance of $4/\kappa$. The Debye length in water is on the order of 3−30 nm for the ionic strength range 10−0.1 mM. The solubility of single ions in oil (or any other low-dielectric medium) is $\sim 10^{-9}$ M, and thus the Debye length in the oil phase is typically ∼1.5 μm. On a planar surface the total charge−charge repulsion/attraction is reduced by half compared to an aqueous bulk solution, since only the water phase contains a significant amount of charge (Figure 3a), and the oil phase is essentially infinite. Thus, charges at a planar interface experience Coulombic repulsion from other co-ions situated in a hemisphere with a radius $\sim 4/\kappa$ adjacent to the interface. Experimental data[26,58,59] show that high charge densities can be obtained for surfactants adsorbed at planar oil/water interfaces. For nanodroplets and nanoparticles that are smaller than $4/\kappa \approx 6$ μm, it can be expected that the electrostatic field from the surface charges will not be screened by the oil (as illustrated in Figure 3b). Every interfacial charge will thus experience the electrostatic repulsion from all other interfacial charges on opposing surfaces through the oil phase and from all the charges in the bulk that are separated by a few Debye lengths in the aqueous phase. As such, the surface charge density will likely be similar to the charge spacing in the aqueous phase.

In order to understand whether the physical picture described above contains the right ingredients, we consider a system in which space is modified into three areas with different dielectric constants and Debye lengths (ε_1, κ_1 for the water phases on the outer sides and ε_2, κ_2 for the oil phase with a

DOI: 10.1021/acsnano.7b05100
ACS Nano 2017, 11, 12111−12120

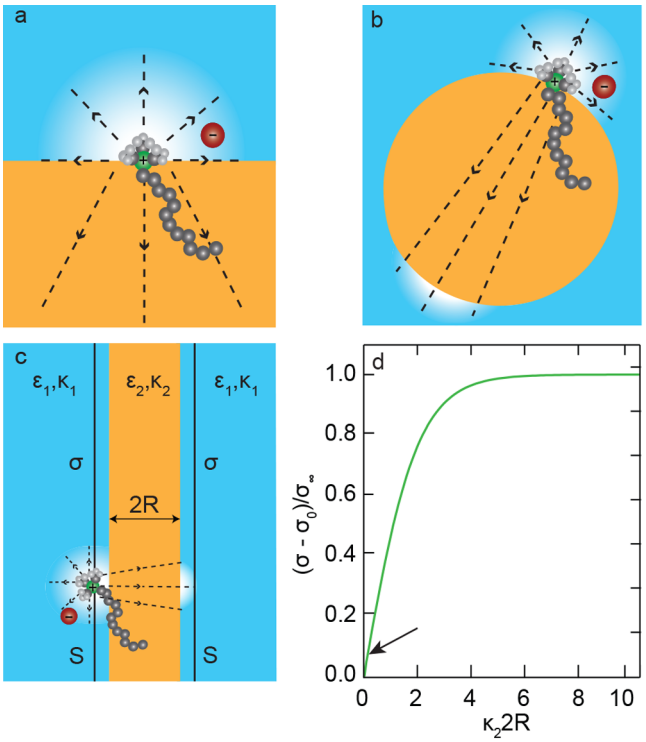

Figure 3. Sketch of the lines of the electrostatic field created by a DTA^+ cation (a) at a single planar interface, (b) on a droplet, and (c) at two opposing planar interfaces. The two regions of water, with dielectric constant ε_1 and Debye screening parameter κ_1, are separated by an intervening region of oil, with dielectric constant ε_2, Debye screening parameter κ_2, depth $2R$, and surface charge density σ. (d) Relative surface charge density σ of the opposing surfaces shown in (c) as a function of R, normalized to the value with $R \to \infty$. σ_0 is the charge density value for $R = 0$ (at the absence of the intervening dielectric) and is used as a reference value. The values used are $\varepsilon_1 = 78$, $\kappa_1 = 0.33$ nm^{-1} ($1/\kappa_1 = 3$ nm), $\varepsilon_2 = 2$, and $\kappa_2 = 0.67$ μm^{-1} ($1/\kappa_2 = 1.49$ μm). The arrow indicates the region of $\kappa_2 2R$ values corresponding to the droplets under study, with radius R in the range 45 nm < R < 125 nm. See the SI for further information about the calculation.

thickness R between the water phases, Figure 3c) and insert two parallel sheets S with surface charge density σ in the water phase, at a distance of 3 Å (the size of a water molecule) away from the oil/water interface, in order to mimic two opposing layers of adsorbate. We calculate the electric potential $V(z)$ by solving the linearized Poisson−Boltzmann equation (where z is the distance perpendicular to the oil/water interfaces). Knowing $V(z)$ we calculate the energy required to create the two charged sheets as a function of σ and the thickness of the oil phase. Setting this energy equal to the thermal energy k_BT, we then obtain an expression for σ in terms of R. Figure 3d shows the relative change $(\sigma - \sigma_0)/\sigma_\infty$ as a function of $\kappa_2 2R$, where σ_0 is the surface charge density at $R = 0$ and σ_∞ the limiting values for large radius ($R \to \infty$). The Debye parameters and dielectric constants used are those discussed in the previous paragraph for water ($\varepsilon_1 = 78$, $\kappa_1 = 0.33$ nm^{-1}, and $1/\kappa_1 = 3$ nm) and hexadecane ($\varepsilon_2 = 2$, $\kappa_2 = 0.67$ μm^{-1}, and $1/\kappa_2 = 1.49$ μm). The experimentally accessed values are $0.06 < \kappa_2 2R < 0.17$ (using the average intensity weighted radii; with larger radii that are also present in the distribution the limiting value would be 0.5). It can be seen that, as the interfaces approach each other, the surface charge density on each sheet decreases, as a consequence of the increasing repulsive interaction between the charges on both sheets. The same trend is observed when changing the interfacial thickness or else the distance of the sheets S from the interface at a constant R: the surface charge density on each sheet decreases as the interfacial thickness decreases. Although this simplistic model does not resemble a droplet interface, it shows that the expected mechanism for the interaction of charges adsorbed to opposing interfaces indeed occurs. This picture implies that in the absence of any interactions stronger than the electrostatic repulsion considered here, the spacing of charges for small enough droplets (*i.e.*, with $R < 3$ μm) should be comparable to the distance of charges in solution. To further test our hypothesis, we compare the Debye length in solution to the interfacial charge spacing and measure changes therein, as a function of ionic strength.

Electrostatic Interactions in Charged Systems. To do so, we prepared 1 vol % suspensions of ~100 nm in radius d_{34}-hexadecane droplets in D_2O, with a constant droplet size and distribution with different amounts of SDS added to the solution (similar to that in Figure 1c, ref 29, SI). Figure 4a

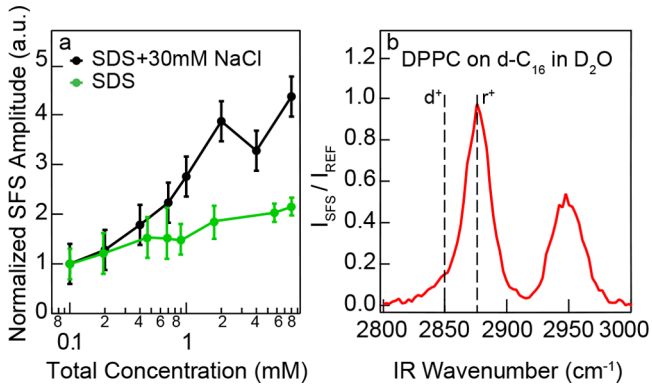

Figure 4. Electrostatic interactions. (a) SFS amplitudes of the S−O symmetric stretch mode of DS^- ions at the interface of d_{34}-hexadecane nanodroplets in D_2O for different SDS concentrations with (black) and without (green) 30 mM NaCl. The SFS spectra were recorded in the range of 1000−1150 cm^{-1}. (b) SFS spectra in the C−H stretch region of DPPC monolayers on 2 vol % d_{34}-hexadecane nanodroplets in D_2O taken for 1 mM of DPPC bulk concentration. The symmetric methylene (d^+ at ~2850 cm^{-1}) and the symmetric methyl (r^+ at ~2876 cm^{-1}) stretch vibrational modes are indicated by the vertical lines. All SFS spectra for (a) and (b) were collected with the IR (vis, SF) beam polarized parallel (perpendicular) to the scattering plane (SSP) and normalized with the DLS size distribution according to the protocol in ref 34.

displays the SFS amplitude of the S−O stretch vibration as a function of the total DS^- concentration in solution without (green) and with (black) the addition of 30 mM NaCl. All values are normalized to the SFS amplitude obtained from the solution with the smallest amount of DS^- ions (100 μM). Without NaCl, the surface density of DS^- anions increases by a factor of ~2 when the DS^- concentration is varied from 100 μm to 8 mM. Thus, a minimum projected surface area of 4.25 nm^2 is reached (at 8 mM), corresponding to an interfacial DS^- spacing of >2.1 nm. Additionally, the Debye length in the bulk solution is ~3 nm. The similarity of the two values is striking and, in the absence of ion pairing,[43] in agreement with the prediction presented above, namely, that the surface charge separation should be similar to the spacing of surfactant

DOI: 10.1021/acsnano.7b05100
ACS Nano 2017, 11, 12111−12120

molecules in the aqueous phase. With 30 mM NaCl and 8 mM SDS ($1/\kappa$ = 1.57 nm), Figure 4a shows that the SFS amplitude increases to a higher value, corresponding to an increased surface density by ~2.2 times at 8 mM, equivalent to a projected surface area of >2.1 nm^2 per DS^- ion. This area corresponds to a surface spacing of >1.5 nm, again close to the Debye length in solution.

Thus, increasing the electrostatic screening in the bulk solution results in an interfacial layer that is more densely packed. Note that higher NaCl concentrations will not lead to even more densely packed films, as this will instead result in more efficient micellization (the cmc for SDS is 3 mM with 30 mM NaCl added to the solution[44]). In addition, the resemblance between the ion spacing at the interface and the Debye length in solution suggests that, indeed, the small droplets do not screen the electrostatic field from interfacial surfactant molecules. Thus, the surfactants experience the same electrostatic field on the droplet surface as in the bulk, and this is expected for all aqueous solutions of nanoparticles that have a low dielectric constant and negligible amount of charged species in their bulk phase. On the contrary, on extended planar interfaces a surfactant molecule close to the interface does not experience any electrostatic field through the oil phase (Figure 3a), while a surfactant molecule in the bulk water experiences the electrostatic field from all surfactant molecules in solution at a distance up to $4/\kappa$. This difference from the nanodroplets is reflected on the ion spacing at the flat interface, which is ~0.7 nm,[57] clearly smaller that the Debye length of ~3 nm. This tight packing is also facilitated by counterion condensation, which is also different for different surface geometries[60] and further reduces the electrostatic repulsion between like charges.

To confirm the importance of counterions, we compare the surface density of DS^-, DTA^+, and hexanol to that of a zwitterionic lipid, 1,2-dipalmitoyl-*sn*-glycero-3-phosphocholine (DPPC). Figure 4b shows the SFS spectrum of the C−H stretch mode region of DPPC lipids adsorbed at the d_{34}-hexadecane/D_2O nanodroplet interface. Comparing the SFS spectra of droplets coated with different amounts of DPPC, and comparing the data to SFG spectra from a DPPC monolayer at the air/water interface with a known surface density, it was found that DPPC can self-assemble to form a dense monolayer with a projected molecular area of 0.48 nm.[57] This confirms that, for the case of charged surfactants that are adsorbed as dissociated charges, there is a net repulsion between the surface ions, which ensures droplet stability, but also reduces the surface density. However, as determined from the above discussion, a high surface density of surfactants (above a certain barrier) is apparently not needed for droplet stability. Indeed, adding NaCl to the emulsion with SDS does not result in a difference in the stability of the nanodroplets, while it does lead to an increase in the surface density of DS^-.

CONCLUSIONS

We have investigated the stability and molecular structure of oil nanodroplets in water that were stabilized with negatively charged, positively charged, neutral, or zwitterionic molecules. We used a combination of methods that report on macroscopic properties and molecular interfacial structures. We find that ionic surfactants are better stabilizers than neutral and zwitterionic ones. Contrary to the general expectation based on geometrical packing, that a good stability is accompanied by a high surface density, the neutral/zwitterionic surfactants have a >15 times higher surface density than the charged surfactants, but the droplets are less stable. Head group hydration influences the orientational ordering of water, which is affected by both charge−dipole interactions and hydrogen bonding. Specifically, hexanol forms hydrogen bonds with water and, as a consequence, there is a polarized layer of weakly oriented water dipoles that provides some stability to the droplets. DTA^+ ions repel each other and form a dilute interfacial layer, with the somewhat hydrophobic cations situated inside the oil. Additionally, there is no hydrogen bonding between DTA^+ and water in this system, but the interfacial water network is disrupted because of charge−dipole interactions. DS^- ions also repel each other, but they form a denser layer than DTA^+, as the water molecules screen the charges more effectively (by combined charge−dipole and hydrogen-bonding interactions). The effect of electrostatic screening on the interfacial structure has been further investigated for DS^- ions by adding NaCl to the solution, which results in more densely packed surfactant layers. The surface spacing of surfactant ions is still comparable to the Debye length in solution. In contrast, charge-neutralized zwitterionic layers do not display this behavior and instead form densely packed monolayers. The latter demonstrates again the important difference between charged and charge neutral surfactants.

The differences between nanoscale interfaces and extended planar interfaces are caused by a difference in charge−charge screening interactions on the submicrometer length scale. For small droplet systems there is less screening in the oil phase, resulting in a lower surface density of free charges. This behavior is generic, extends up to the micrometer-scale, and is thus expected to occur for any type of dielectric particle in water. It is also expected to occur for the inverse system of water droplets in oil.

MATERIALS AND METHODS

Chemicals. *n*-Hexadecane ($C_{16}H_{34}$, 99.8%, Sigma-Aldrich), d_{34}-hexadecane ($C_{16}D_{34}$, 98% d, Cambridge Isotope), *h*-sodium dodecyl sulfate (99%, Biomol), d-SDS (99% d, Cambridge Isotope), *h*-dodecyltrimethylammonium bromide (99%, Sigma-Aldrich), d-DTAB (99% d, Cambridge Isotope), 1-hexanol ($CH_3(CH_2)_5OH$, 99.5%, Sigma-Aldrich), 1-hexan-d_{13}-ol ($CD_3(CD_2)_5OH$, 98% d, Sigma-Aldrich), 1,2-dipalmitoyl-*sn*-glycero-3-phosphocholine (99%, Avanti), sodium chloride (NaCl, 99.999%, Acros Organics), sodium bromide (NaBr, 98.52%, J.T. Baker), trimethyloctylammonium bromide (OTA^+, ≥98.0%, Sigma-Aldrich), sodium octylsulfate (SOS, ~95% Sigma-Aldrich), and D_2O (99.8%, Armar, >2 MΩ cm) were used as received. Aqueous solutions of amphiphiles and salts were prepared using ultrapure water (H_2O, Milli-Q UF Plus, Millipore, Inc., electrical resistance of 18.2 MΩ cm, D_2O, 99.8%, Armar, >2 MΩ cm). All glassware was cleaned with a solution of 3:7 H_2O_2/H_2SO_4 and subsequently was thoroughly rinsed with ultrapure water.

Emulsion Preparation. In order to achieve the demanded concentrations of oil, surfactant, and salt (Figures 1, 2a,b, and 4a), stock dispersions of oil nanodroplets in water were prepared with 1, 1.5, or 2 vol % of hexadecane or d_{34}-hexadecane in D_2O (for SFS) or H_2O (for SHS). Subsequently they were diluted with solutions of appropriate concentrations of SDS, DTAB, or hexanol and a solution of NaCl (only in Figure 4a) in D_2O or H_2O. In this way the size distribution of nanodroplets was kept constant between samples stabilized with the same surfactant. For the preparation of the stock solutions, the oil-in-water dispersions were mixed for 2 min with a hand-held homogenizer (TH, OMNI International) of angular velocity of 15 rpm and then placed in an ultrasonic bath (35 kHz, 400 W, Bandelin) for 5 to 10 min. The size distribution of the droplets was measured with dynamic light scattering (Malvern ZS nanosizer) and, for stable samples, was consistently found to have a mean radius in the range of 45−125 nm with a PDI of less than 0.2. In the case of DPPC

DOI: 10.1021/acsnano.7b05100
ACS Nano 2017, 11, 12111−12120

(Figure 4b), a lipid monolayer on oil nanodroplets in water was prepared with 2 vol % of hexadecane or d_{34}-hexadecane in D_2O (for SFS) or H_2O (for SHS). The solutions were mixed at a temperature of 45 °C (above the transition temperature of 41 °C for DPPC) with 1 mM of DPPC powder using the above-mentioned homogenizer for 4 min and ultrasonic bath for the same duration. The dispersion had an average radius of 110 nm and a PDI of less than 0.2. The hydrodynamic radii were calculated from the intensity autocorrelation function, using the optical properties of the liquids (hexadecane, d_{34}-hexadecane, and D_2O). The samples were stored and measured in sealed cuvettes. All measurements were performed at 24 °C. The resultant droplet system was used for SFS measurements and was diluted to 0.1 vol % of hexadecane with pure water for SHS measurements. All data were recorded using, for each surfactant, the same droplet stock sample, excluding variations in droplet size distribution.[29]

Second-Harmonic Scattering. For second-harmonic scattering measurements, the setup has been previously described in detail in ref 61. Incoming laser pulses of 190 fs centered at 1028 nm with a 200 kHz repetition rate were filtered with a long pass filter (FEL0750, Thorlabs) and focused by a plano-convex lens (f = 7.5 cm) into a cylindrical glass sample cell of inner diameter of 4.2 mm. Their polarization was controlled by a Glan-Taylor polarizer (GT10-B, Thorlabs) and a zero-order half-wave plate (WPH05M-1030). The scattered SH light was collected with an iris of 10 mm diameter (acceptance angle of 11.4°), collimated by a plano-convex lens (f = 5 cm), and focused by a second plano-convex lens (f = 3 cm) on a photon multiplier tube (H7421-40, Hamamatsu). The measurement was taken with a gate width of 10 ns and acquisition time of 1 s. The measured light was filtered with a band-pass filter (ET525/50, Chroma), and its polarization direction was selected by a Glan−Taylor polarizer (GT10-A, Thorlabs). The maximum SH intensities were measured for a scattering angle of 35°. The plotted data were normalized to the PP signal of neat water:

$$\frac{I(\theta = 35^\circ)_{\mathrm{SHS,droplets,PPP}} - I(\theta = 35^\circ)_{\mathrm{HRS,solution,PPP}}}{I(\theta = 35^\circ)_{\mathrm{HRS,water,PPP}}}$$

The reproducibility of the SHS measurements is in the range of 1−2%. All data points were acquired with a 50 × 1 s acquisition time.

Sum Frequency Scattering. For vibrational sum frequency scattering measurements, the setup has been previously described in detail in refs 48 and 62. An infrared (IR) and a visible (vis) laser beam were temporally and specially overlapped under an angle of 20° (measured in air) in a sample cuvette with a path length of 200 μm. The IR pulses were centered at 2900 cm^{-1} (fwhm = 160 cm^{-1}) for the measurement of C−H stretch vibrational modes and at 1080 cm^{-1} (fwhm = 120 cm^{-1}) for the measurement of S−O vibrational modes, and the vis pulses at 12 500 cm^{-1} (fwhm = 12 cm^{-1}) at a repetition rate of 1 kHz. The polarization of the IR beam was controlled by two BaF_2 wire grid polarizers (Thorlabs, WP25H-B), while of the vis beam by a polarizing beam splitter cube (CVI, PBS-800-050) and a half-wave plate (EKSMA, 460-4215). The SFS light was measured at a scattering angle of 57°, collected and collimated by a plano-convex lens (f = 15 mm, Thorlabs LA1540-B). Subsequently the polarization state of the SFS light was controlled by a Glan−Taylor prism (Thorlabs, GT15-B), and it was filtered by two short wave pass filters (3rd Millenium, 3RD770SP). Finally it was spectrally dispersed with a monochromator (Acton, SpectraPro 2300i) and detected with an intensified CCD camera (Princeton Instruments, PI-Max3). The gate width was set to 10 ns, and the acquisition time for a single spectrum between 150 and 300 s. All SFS spectra shown were normalized by an SFG spectrum obtained in reflection geometry from a z-cut quartz crystal. For the concentration series a reference sample was measured between every other measurement to detect and correct for possible fluctuations during the course of the experiment.

Raman Hydration Shell Spectroscopy. For the acquisition of Raman hydration shell spectra, the experimental setup and the measurement analysis have been presented before (see SI of ref 54 and the references therein). Briefly, an argon-ion laser centered at 514.5 nm was used as the excitation source, with approximately 15 mW of power at the sample. Duplicate spectra were collected with an integration time of 5 min. The backscattered Raman photons were collected and delivered at the entrance slit of a 300 gr/mm-grating using a fiber bundle consisting of seven 100 μm core diameter fibers (arranged in a close packed circular array at the collection end and a linear stack at the entrance slit). The spectral resolution of the Raman system is estimated as ∼1 nm (∼25 cm^{-1} or ∼4 CCD pixels). All Raman spectra are unpolarized, including both S and P polarized scattering. The Raman-MCR decomposition of measured spectra into SC and pure water components was performed using self-modeling curve resolution by keeping the Br^- concentration the same in both solvent (as Na^+Br^-) and OTA^+ surfactant solutions (as OTA^+Br^-).[63,64] Since the O−H stretch signature of water molecules around Na^+ ions is virtually indistinguishable from that of pure water,[65] Na^+ ions have essentially no influence on the above SC spectra or those obtained from OS^-Na^+ surfactant solutions (with salt-free water as the solvent).

ASSOCIATED CONTENT

Supporting Information

The Supporting Information is available free of charge on the ACS Publications website at DOI: 10.1021/acsnano.7b05100.

Theoretical calculation of the relative change of the surface charge density of two infinite parallels sheets that are situated on the two sides of an oil layer, which is surrounded by water on both sides, as a function of the thickness of the oil layer; the calculation is based on a solution of the linearized Poisson−Boltzmann equation (PDF)

AUTHOR INFORMATION

Corresponding Author

*E-mail: sylvie.roke@epfl.ch.

ORCID

Yixing Chen: 0000-0001-8492-9615
Halil I. Okur: 0000-0002-2492-1168
Sylvie Roke: 0000-0002-6062-7871

Author Contributions

E.Z. and Y.C. performed experimental measurements and reproducibility validations. E.Z., Y.C., H.I.O., and S.R. performed analytical analysis, and S.R., E.Z., and H.I.O. wrote the manuscript. D.M.W. performed the modeling for Figure 3. S.R. conceived and supervised the work.

Notes

The authors declare no competing financial interest.

ACKNOWLEDGMENTS

This work is supported by the Julia Jacobi Foundation, the Swiss National Science Foundation (grant number 200021_140472), and the European Research Council (grant numbers 240556 and 616305). We thank B. M. Ranking and D. Ben-Amotz for making Raman hydration shell data available to us.

REFERENCES

(1) Hunter, R. J. *Foundations of Colloid Science*; Oxford University Press: New York, 2001.

(2) McClements, J. D. Critical Review of Techniques and Methodologies for Chararacterization of Emulsion Stability. *Crit. Rev. Food Sci. Nutr.* **2007**, *47*, 611−649.

DOI: 10.1021/acsnano.7b05100
ACS Nano 2017, 11, 12111−12120

(3) Mason, T. G.; Wilking, J. N.; Meleson, K.; Chang, C. B.; Graves, S. M. Nanoemulsions: Formation, Structure, and Physical Properties. *J. Phys.: Condens. Matter* **2006**, *18*, R635−R666.
(4) Taly, V.; Kelly, B. T.; Griffiths, A. D. Droplets as Microreactors for High-Throughput Biology. *ChemBioChem* **2007**, *8*, 263−272.
(5) Teh, S.-Y.; Lin, R.; Hung, L.-H.; Lee, A. P. Droplet Microfluidics. *Lab Chip* **2008**, *8*, 198−220.
(6) Seemann, R.; Brinkmann, M.; Pfohl, T.; Herminghaus, S. Droplet Based Microfluidics. *Rep. Prog. Phys.* **2012**, *75*, 016601.
(7) Guo, M. T.; Rotem, A.; Heyman, J. A.; Weitz, D. A. Droplet Microfluidics for High-Throughput Biological Assays. *Lab Chip* **2012**, *12*, 2146−2155.
(8) Amstad, E.; Gopinadhan, M.; Holtze, C.; Osuji, C. O.; Brenner, M. P.; Spaepen, F.; Weitz, D. A. Production of Amorphous Nanoparticles by Supersonic Spray-Drying with a Microfluidic Nebulator. *Science* **2015**, *349*, 956−960.
(9) Grzybowski, B. A.; Huck, W. T. S. The Nanotechnology of Life-Inspired Systems. *Nat. Nanotechnol.* **2016**, *11*, 585−592.
(10) Miller, O. J.; Harrak, A. E.; Mangeat, T.; Baret, J.-C.; Frenz, L.; Debs, B. E.; Mayot, E.; Samuels, M. L.; Rooney, E. K.; Dieu, P.; Galvan, M.; Link, D. R.; Griffiths, A. D. High-Resolution Dose−Response Screening Using Droplet-Based Microfluidics. *Proc. Natl. Acad. Sci. U. S. A.* **2012**, *109*, 378−383.
(11) Pekin, D.; Skhiri, Y.; Baret, J.-C.; Le Corre, D.; Mazutis, L.; Ben Salem, C.; Millot, F.; El Harrak, A.; Hutchison, J. B.; Larson, J. W.; Link, D. R.; Laurent-Puig, P.; Griffiths, A. D.; Taly, V. Quantitative and Sensitive Detection of Rare Mutations Using Droplet-Based Microfluidics. *Lab Chip* **2011**, *11*, 2156−2166.
(12) Debs, B. E.; Utharala, R.; Balyasnikova, I. V.; Griffiths, A. D.; Merten, C. A. Functional Single-Cell Hybridoma Screening Using Droplet-Based Microfluidics. *Proc. Natl. Acad. Sci. U. S. A.* **2012**, *109*, 11570−11575.
(13) Sjostrom, S. L.; Bai, Y.; Huang, M.; Liu, Z.; Nielsen, J.; Joensson, H. N.; Andersson Svahn, H. High-Throughput Screening for Industrial Enzyme Production Hosts by Droplet Microfluidics. *Lab Chip* **2014**, *14*, 806−813.
(14) Fischer, E. K.; Harkins, W. D. Monomolecular Films, the Liquid-Liquid Interface and the Stability of Emulsions. *J. Phys. Chem.* **1932**, *36*, 98−110.
(15) Israelachvili, J. N. *Intermolecular and Surface Forces*; Academic Press: San Diego, 2011.
(16) Atkins, P.; de Paula, J. *Atkins' Physical Chemistry*; Oxford University Press: Oxford, 2010.
(17) Lyklema, J. *Fundamentals of Interface and Colloid Science: Soft Colloids*; Elsevier Science: Amsterdam, 2005.
(18) Adamson, A. W.; Gast, A. P. *Physical Chemistry of Surfaces*; Wiley: New York, 1997.
(19) Als-Nielsen, J.; McMorrow, D. *Elements of Modern X-ray Physics*; Wiley: Hoboken, 2011.
(20) Berge, B.; Konovalov, O.; Lajzerowicz, J.; Renault, A.; Rieu, J. P.; Vallade, M.; Als-Nielsen, J.; Grubel, G.; Legrand, J. F. Melting of Short 1-Alcohol Monolayers on Water: Thermodynamics and X-ray Scattering Studies. *Phys. Rev. Lett.* **1994**, *73*, 1652−1655.
(21) Lu, J. R.; Marrocco, A.; Su, T. J.; Thomas, R. K.; Penfold, J. Adsorption of Dodecyl Sulfate Surfactants with Monovalent Metal Counterions at the Air-Water Interface Studied by Neutron Reflection and Surface Tension. *J. Colloid Interface Sci.* **1993**, *158*, 303−316.
(22) Sloutskin, E.; Sapir, Z.; Bain, C. D.; Lei, Q.; Wilkinson, K. M.; Tamam, L.; Deutsch, M.; Ocko, B. M. Wetting, Mixing, and Phase Transitions in Langmuir-Gibbs Films. *Phys. Rev. Lett.* **2007**, *99*, 136102−136104.
(23) Guyot-Sionnest, P.; Hunt, J. H.; Shen, Y. R. Sum-Frequency Vibrational Spectroscopy of a Langmuir Film: Study of Molecular-Orientation of a Two Dimensional System. *Phys. Rev. Lett.* **1987**, *59*, 1597−1600.
(24) Harris, A. L.; Chidsey, C. E. D.; Levinos, N. J.; Loiacona, D. N. Monolayer Vibrational Spectroscopy by Infrared-Visible Sum Generation at Metal and Semiconductor Surfaces. *Chem. Phys. Lett.* **1987**, *141*, 350−356.
(25) Conboy, J. C.; Messmer, M. C.; Richmond, G. L. Dependence of Alkyl Chain Conformation of Simple Ionic Surfactants on Head Group Functionality as Studied by Vibrational Sum-Frequency Spectroscopy. *J. Phys. Chem. B* **1997**, *101*, 6724−6733.
(26) Knock, M. M.; Bell, G. R.; Hill, E. K.; Turner, H. J.; Bain, C. D. Sum-Frequency Spectroscopy of Surfactant Monolayers at the Oil-Water Interface. *J. Phys. Chem. B* **2003**, *107*, 10801−10814.
(27) Messmer, M. C.; Conboy, J. C.; Richmond, G. L. Observation of Molecular Ordering at the Liquid-Liquid Interface by Resonant Sum-Frequency Generation. *J. Am. Chem. Soc.* **1995**, *117*, 8039−8040.
(28) Richmond, G. L. Structure and Bonding of Molecules at Aqueous Surfaces. *Annu. Rev. Phys. Chem.* **2001**, *52*, 357−389.
(29) de Aguiar, H. B.; de Beer, A. G. F.; Strader, M. L.; Roke, S. The Interfacial Tension of Nanoscopic Oil Droplets in Water Is Hardly Affected by SDS Surfactant. *J. Am. Chem. Soc.* **2010**, *132*, 2122−2123.
(30) Smolentsev, N.; Smit, W. J.; Bakker, H. J.; Roke, S. The Interfacial Structure of Water Droplets in a Hydrophobic Liquid. *Nat. Commun.* **2017**, *8*, 15548.
(31) Kurylowicz, M.; Paulin, H.; Mogyoros, J.; Giuliani, M.; Dutcher, J. R. The Effect of Nanoscale Surface Curvature on the Oligomerization of Surface-Bound Proteins. *J. R. Soc., Interface* **2014**, *11*, 1−9.
(32) Jackson, A. M.; Myerson, J. W.; Stellacci, F. Spontaneous Assembly of Subnanometre-Ordered Domains in the Ligand Shell of Monolayer-Protected Nanoparticles. *Nat. Mater.* **2004**, *3*, 330−336.
(33) Long, J. A.; Rankin, B. M.; Ben-Amotz, D. Micelle Structure and Hydrophobic Hydration. *J. Am. Chem. Soc.* **2015**, *137*, 10809−10815.
(34) Smolentsev, N.; Lütgebaucks, C.; Okur, H. I.; de Beer, A. G. F.; Roke, S. Intermolecular Headgroup Interaction and Hydration as Driving Forces for Lipid Transmembrane Asymmetry. *J. Am. Chem. Soc.* **2016**, *138*, 4053−4060.
(35) Roke, S.; Roeterdink, W. G.; Wijnhoven, J. E. G. J.; Petukhov, A. V.; Kleyn, A. W.; Bonn, M. Vibrational Sum Frequency Scattering from a Submicron Suspension. *Phys. Rev. Lett.* **2003**, *91*, 258302.
(36) Roke, S.; Gonella, G. Nonlinear Light Scattering and Spectroscopy of Particles and Droplets in Liquids. *Annu. Rev. Phys. Chem.* **2012**, *63*, 353−378.
(37) Schürer, B.; Wunderlich, S.; Sauerbeck, C.; Peschel, U.; Peukert, W. Probing Colloidal Interfaces by Angle-Resolved Second Harmonic Light Scattering. *Phys. Rev. B: Condens. Matter Mater. Phys.* **2010**, *82*, 241404−241404.
(38) Wang, H.; Yan, E. C. Y.; Borguet, E.; Eisenthal, K. B. Second Harmonic Generation from the Surface of Centrosymmetric Particles in Bulk Solution. *Chem. Phys. Lett.* **1996**, *259*, 15−20.
(39) de Aguiar, H. B.; Samson, J. S.; Roke, S. Probing Nanoscopic Droplet Interfaces in Aqueous Solution with Vibrational Sum-Frequency Scattering: A Study of the Effects of Path Length, Droplet Density and Pulse Energy. *Chem. Phys. Lett.* **2011**, *512*, 76−80.
(40) de Beer, A. G. F.; Roke, S. Obtaining Molecular Orientation from Second Harmonic and Sum Frequency Scattering Experiments in Water: Angular Distribution and Polarization Dependence. *J. Chem. Phys.* **2010**, *132*, 234702.
(41) Johansson, P. K.; Koelsch, P. Vibrational Sum-Frequency Scattering for Detailed Studies of Collagen Fibers in Aqueous Environments. *J. Am. Chem. Soc.* **2014**, *136*, 13598−13601.
(42) Petersen, P. B.; Saykally, R. J. Probing the Interfacial Structure of Aqueous Electrolytes with Femtosecond Second Harmonic Generation Spectroscopy. *J. Phys. Chem. B* **2006**, *110*, 14060−14073.
(43) Scheu, R.; Chen, Y.; Subinya, M.; Roke, S. Stern Layer Formation Induced by Hydrophobic Interactions: A Molecular Level Study. *J. Am. Chem. Soc.* **2013**, *135*, 19330−19335.
(44) Mukerjee, P. M. K. J. Critical Micelle Concentrations of Aqueous Surfactant Systems. *Natl. Stand. Ref. Data Ser. (U. S., Natl. Bur. Stand.)* **1971**, *36*, 1−222.
(45) Stephenson, R.; Stuart, J.; Tabak, M. Mutual Solubility of Water and Aliphatic Alcohols. *J. Chem. Eng. Data* **1984**, *29*, 287−290.
(46) Chen, Y.; Jena, K. C.; Roke, S. From Hydrophobic to Hydrophilic: The Structure and Density of the Hexadecane

DOI: 10.1021/acsnano.7b05100
ACS Nano 2017, 11, 12111−12120

Droplet/Alkanol/Water Interface. *J. Phys. Chem. C* **2015**, *119*, 17725−17734.
(47) Wang, H. F.; Yan, E. C. Y.; Liu, Y.; Eisenthal, K. B. Energetics and Population of Molecules at Microscopic Liquid and Solid Surfaces. *J. Phys. Chem. B* **1998**, *102*, 4446−4450.
(48) de Aguiar, H. B.; Strader, M. L.; de Beer, A. G. F.; Roke, S. Surface Structure of Sodium Dodecyl Sulfate Surfactant and Oil at the Oil-in-Water Droplet Liquid/Liquid Interface: A Manifestation of a Non-Equilibrium Surface State. *J. Phys. Chem. B* **2011**, *115*, 2970−2978.
(49) Cederquist, K. B.; Keating, C. D. Curvature Effects in DNA:Au Nanoparticle Conjugates. *ACS Nano* **2009**, *3*, 256−260.
(50) Hunter, R. J. *Zeta Potential in Colloid Science: Principles and Applications*; Academic Press: San Diego, 1981.
(51) Scheu, R.; Chen, Y.; de Aguiar, H. B.; Rankin, B. M.; Ben-Amotz, D.; Roke, S. Specific Ion Effects in Amphiphile Hydration and Interface Stabilization. *J. Am. Chem. Soc.* **2014**, *136*, 2040−2047.
(52) Vacha, R.; Roke, S. Sodium Dodecyl Sulfate at Water-Hydrophobic Interfaces: A Simulation Study. *J. Phys. Chem. B* **2012**, *116*, 11936−11942.
(53) Scheu, R.; Rankin, B. M.; Chen, Y.; Jena, K. C.; Ben-Amotz, D.; Roke, S. Charge Asymmetry at Aqueous Hydrophobic Interfaces and Hydration Shells. *Angew. Chem., Int. Ed.* **2014**, *53*, 9560−9563.
(54) Davis, J. G.; Gierszal, K. P.; Wang, P.; Ben-Amotz, D. Water Structural Transformation at Molecular Hydrophobic Interfaces. *Nature* **2012**, *491*, 582−585.
(55) Fega, K. R.; Wilcox, D. S.; Ben-Amotz, D. Application of Raman Multivariate Curve Resolution to Solvation-Shell Spectroscopy. *Appl. Spectrosc.* **2012**, *66*, 282−288.
(56) Fayer, M. D.; Levinger, N. E. Analysis of Water in Confined Geometries and at Interfaces. *Annu. Rev. Anal. Chem.* **2010**, *3*, 89−107.
(57) Rehfeld, S. J. Adsorption of Sodium Dodecyl Sulfate at Various Hydrocarbon-Water Interfaces. *J. Phys. Chem.* **1967**, *71*, 738−745.
(58) Möhwald, H. Surfactant Layers at Water Surfaces. *Rep. Prog. Phys.* **1993**, *56*, 653.
(59) Schlossman, M. L.; Tikhonov, A. M. Molecular Ordering and Phase Behavior of Surfactants at Water-Oil Interfaces as Probed by X-Ray Surface Scattering. *Annu. Rev. Phys. Chem.* **2008**, *59*, 153−177.
(60) Manning, G. S. Counterion Condensation on Charged Spheres, Cylinders, and Planes. *J. Phys. Chem. B* **2007**, *111*, 8554−8559.
(61) Gomopoulos, N.; Lütgebaucks, C.; Sun, Q. C.; Macias-Romero, C.; Roke, S. Label-Free Second Harmonic and Hyper Rayleigh Scattering with High Efficiency. *Opt. Express* **2013**, *21*, 815−821.
(62) de Aguiar, H. B.; Scheu, R.; Jena, K. C.; de Beer, A. G. F.; Roke, S. Comparison of Scattering and Reflection SFG: A Question of Phase-Matching. *Phys. Chem. Chem. Phys.* **2012**, *14*, 6826−6832.
(63) Davis, J. G.; Rankin, B. M.; Gierszal, K. P.; Ben-Amotz, D. On the Cooperative Formation of Non-Hydrogen-Bonded Water at Molecular Hydrophobic Interfaces. *Nat. Chem.* **2013**, *5*, 796−802.
(64) Rankin, B. M.; Ben-Amotz, D. Expulsion of Ions from Hydrophobic Hydration Shells. *J. Am. Chem. Soc.* **2013**, *135*, 8818−8821.
(65) Perera, P. N.; Browder, B.; Ben-Amotz, D. Perturbations of Water by Alkali Halide Ions Measured Using Multivariate Raman Curve Resolution. *J. Phys. Chem. B* **2009**, *113*, 1805−1809.

DOI: 10.1021/acsnano.7b05100
ACS Nano 2017, 11, 12111−12120